

Switching control for tracking of a hybrid position-force trajectory

D.J.F. Heck, A. Saccon, N. van de Wouw, H. Nijmeijer

Eindhoven University of Technology, Department of Mechanical Engineering, P.O. Box 513, NL 5600 MB Eindhoven, The Netherlands

Abstract

This work proposes a control law for a manipulator with the aim of realizing desired time-varying motion-force profiles in the presence of a stiff environment. In many cases, the interaction with the environment affects only one degree of freedom of the end-effector of the manipulator. Therefore, the focus is on this contact degree of freedom, and a switching position-force controller is proposed to perform the hybrid position-force tracking task. Sufficient conditions are presented to guarantee input-to-state stability of the switching closed-loop system with respect to perturbations related to the time-varying desired motion-force profile. The switching occurs when the manipulator makes or breaks contact with the environment. The analysis shows that to guarantee closed-loop stability while tracking arbitrary time-varying motion-force profiles, the controller should implement a considerable (and often unrealistic) amount of damping, resulting in inferior tracking performance. Therefore, we propose to redesign the manipulator with a compliant wrist. Guidelines are provided for the design of the compliant wrist while employing the designed switching control strategy, such that stable tracking of a motion-force reference trajectory can be achieved and bouncing of the manipulator while making contact with the stiff environment can be avoided. Finally, numerical simulations are presented to illustrate the effectiveness of the approach.

Key words: Manipulator control, Motion tracking, Force tracking, Switched system, Model reduction

1 Introduction

Numerous applications such as, e.g., bilateral teleoperation, automated assembly tasks, and surface finishing involve the interaction between a robot manipulator and a stiff environment. In those applications, the stability of transitions from free motion to constrained motion and from constrained motion to free motion is essential for accomplishing the desired task. Ensuring stability during these transitions is a challenge as the combined robot-environment dynamics switches abruptly at the moment of contact and detachment from the environment.

Different control architectures have been proposed for motion-force control of a manipulator in contact (for an overview, see, e.g., [1, Chapter 7]), but the stability question is still open. The most studied and applied control schemes include stiffness, impedance and admittance control [2,3,4,5,6,7], hybrid position-force control [8,9], and parallel position-force control [10]. The gains

in these control schemes are tuned separately for free motion and constrained motion. Stability of the resulting closed-loop dynamics is analyzed using standard Lyapunov methods and guaranteed for free motion and constrained motion, but the contact and detachment transitions are not included in the analysis. Bouncing and unstable contact behavior might therefore still occur, and do still occur. As a practical solution, when implementing these control schemes on a physical manipulator, the manipulator is usually commanded to approach the environment with a very slow velocity to prevent the excitation of the unstable contact dynamics.

The aim of this paper is to go beyond the current state of the art and propose a novel stability analysis for this problem. We propose a mathematical analysis that can help control engineers as well as mechanical designers to develop controlled manipulators that exhibit stable contact behavior with a stiff environment. We propose a controller and a stability analysis to verify if stability is guaranteed even during contact and detachment phases. A key aspect is that we are interested in tracking *time-varying* motion and force profiles. This specific goal originates from our interest in telerobotics, where a force and position reference from the master device has to be translated into a command for the slave device.

* This research is supported by the Dutch Technology Foundation (STW). This paper was not presented at any IFAC meeting. Corresponding author D.J.F. Heck

Email address: d.j.f.heck@tue.nl (D.J.F. Heck).

As the force and position reference comes from a human operator, we want to allow those reference signals to be as general as possible.

Few theoretical studies have addressed directly the root cause of the instability during bouncing against a stiff environment. In [11,12], a switched position-force controller is considered, where the controller switches from motion to force control when contact with the environment is made. Using analysis techniques for switched systems, conditions for asymptotic stability are derived for a *constant* position or force setpoint regulation problem. Hysteresis switching is considered in [13] to prevent bouncing of the manipulator against the environment. In [6], a switching rule is designed for the impedance parameters to dissipate the kinetic energy engaged at impact. The resulting “active impedance control” guarantees “velocity regulation in free motion, impact attenuation” and tracking of a *constant* force setpoint in contact. The number of bounces is cleverly minimized in [14] by exploiting a transition controller, but then the contact force is controlled to a *constant* setpoint. In [15], nonlinear damping is proposed to minimize the force overshoot without compromising the settling time. In all these publications, tracking of desired *time-varying* motion and force profiles is not considered.

In the above mentioned papers, the manipulator-environment interaction is modeled using a flexible spring-damper contact model. The stiffness and damping properties of the environment are included explicitly and, as a consequence, the impact phase has a finite time duration. Such a modeling approach is also taken in this paper.

Manipulator-environment interaction can also be modeled using tools from nonsmooth mechanics [16,17]. In doing so, the time duration of the impact event is assumed to be zero and an impact law (e.g., Newton’s law of restitution) is employed to characterize the collision. Stable tracking of specific force/position profiles using such nonsmooth mechanics modeling formalism has been addressed in this context. In [18], a discontinuous control scheme is proposed to ensure stable regulation on the surface of the unilateral constraint. A switched motion-force tracking controller for manipulators subject to unilateral constraints is considered in [19,20,21]. There, it is shown that the design of the desired trajectory in the transition phase is crucial for achieving stability.

To the best of authors’ knowledge, the problem of stable tracking of arbitrary force/position profiles as we consider in this work has not been solved even in the framework of nonsmooth mechanics. The stability of the tracking controller cast in this framework is clearly of interest and deserves further investigation. This framework will not be addressed here just because, as we mentioned, we adopt a flexible (spring-damper) contact model.

In this work, we propose a control law for making a manipulator track a *time-varying* motion and force

profile. Because in many tasks of practical interest the interaction of the robot end-effector with the environment occurs just in one direction, we study the contact stability problem using a 1-DOF dynamic manipulator model. The remaining unconstrained DOFs can be controlled with standard motion control techniques (see [22]). We propose a switched motion-force tracking control strategy and include the transitions from free motion to contact (and vice versa) in the stability analysis of the closed-loop dynamics. The obtained stability conditions are given in Theorem 1 in Section 3. The stability analysis of the closed-loop system reveals that the controller should implement a considerable amount of damping to guarantee stability while tracking an arbitrary time-varying motion-force profile. Because an excessive amount of damping limits the tracking performance due to a sluggish response, we propose an alternative mechanical manipulator design by including a compliant wrist. In this way, the resonance frequency of the impact and contact transients can be reduced and the associated energy can be dissipated in a passive way. The use of such an “energy absorbing component” is mentioned in [3], but a stability analysis is not considered therein.

The main contributions of this paper are as follows. First, we propose a combination of the compliant wrist design with a novel switched motion-force controller for the tracking of time-varying motion and force profiles. Secondly, we propose a stability analysis that provides design guidelines for both the compliant wrist and controller to guarantee stable contact while tracking arbitrary motion and force profiles. In particular, we show how bouncing of the manipulator against the stiff environment can be prevented without the need of a considerable amount of damping from the controller.

This article is organized as follows. In Section 2, the manipulator and environment model are introduced and the controller design is proposed. The stability analysis is described in Section 3. Section 4 illustrates the obtained results by means of a simulation study. Section 5 discusses the benefits of additional (wrist-)compliance in the manipulator and the conclusions are presented in Section 6.

2 System modeling and controller design

Our primary goal is to design a controller for making a manipulator track a desired motion-force profile. As explained in the introduction, we focus on a 1-DOF modeling of the manipulator-environment interaction.

Consider the decoupled contact DOF of the manipulator as depicted in Figure 1. The Cartesian space dynamics are described by

$$M\ddot{x} + b\dot{x} = F_c - F_e, \quad (1)$$

where x represents the manipulator position, $M > 0$ the equivalent mass of the manipulator, $b > 0$ the viscous friction in the joint, F_c the control force and F_e the force

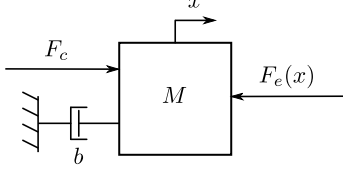


Figure 1. 1-DOF manipulator.

exchanged between the environment and the manipulator. The environment is modeled as a static wall at $x = 0$ and, without loss of generality, the manipulator is in contact with the environment for $x > 0$. In [11,12], the environment is modeled as a piecewise linear spring. We consider, similarly to [13], an extended model including damping and friction. Namely, we use the Kelvin-Voigt contact model

$$F_e(x, \dot{x}) = \begin{cases} 0 & \text{for } x \leq 0 \\ k_e x + b_e \dot{x} & \text{for } x > 0 \end{cases} \quad (2)$$

with $k_e > 0$ and $b_e > 0$ the stiffness and damping properties of the environment, respectively. This model is nonlinear and non-smooth due to the abrupt change in F_e at $x = 0$.

In free motion, the manipulator is required to follow a bounded desired motion profile $x_d(t)$, whereas in contact, a desired force profile $F_d(t)$ should be applied to the environment. Impedance controllers have been proposed in, e.g., [4,5] to control the contact force F_e by creating a force loop around an inner motion control loop. In this way, a desired impedance of the contact is designed, but the contact force is controlled indirectly. We propose, instead, the following switched motion-force controller that switches between a resolved acceleration controller in free motion and a force controller in the contact phase:

$$F_c = \begin{cases} M_a \ddot{x}_d(t) + k_d(\dot{x}_d(t) - \dot{x}) + k_p(x_d(t) - x), & \forall x \leq 0, (3a) \\ F_d(t) + k_f(F_d(t) - F_e) - b_f \dot{x}, & \forall x > 0, (3b) \end{cases}$$

such that both motion and force are controlled directly. Here, $k_p > 0$ and $k_d > 0$ are the proportional and derivative gains of the motion controller, respectively. The estimated mass of the manipulator $M_a > 0$ in (3a) might differ from the actual mass M in (1) due to uncertainties in the model parameter identification. The gain $k_f > 0$ represents the proportional term of the force controller and $b_f > 0$ is the damping gain, dissipating energy during the contact phase. For the controller (3), it is assumed that the contact force F_e , position x and velocity \dot{x} can be measured. Although, in (3), the switching between motion control and force control is decided based on the actual position x of the manipulator, for a stiff environment, $k_e \gg b_e$, this is equivalent to switching based on the interaction force F_e . This implies that a perfect knowledge of the location of the environment is not necessary for the implementation of the controller defined by (3).

In order to analyze stability of the system described by (1)-(3), we reformulate the closed-loop dynamics as a switching state-space model. A key idea for the stability analysis, detailed in Section 3, is to express the force tracking error $F_d(t) - F_e$ in terms of the motion tracking error $x_d(t) - x$, such that both in free motion and in contact the goal is to make the tracking error $x_d(t) - x$ small. In contact, $x_d(t)$ then represents the 'virtual' desired trajectory, corresponding to the desired contact force $F_d(t)$. For the relationship between $F_d(t)$ and $x_d(t)$ during contact, $x \rightarrow x_d(t)$ should also imply $F_e \rightarrow F_d(t)$. To this end, we consider the following relationship to deduce $x_d(t)$ from $F_d(t)$ in the contact phase:

$$\hat{k}_e x_d(t) + \hat{b}_e \dot{x}_d(t) = F_d(t), \quad \text{for } F_d(t) > 0, \quad (4)$$

where \hat{k}_e and \hat{b}_e are available estimates of k_e and b_e .

Assumption 1 *The desired position $x_d(t)$ and velocity $\dot{x}_d(t)$ trajectories are continuous, and the desired acceleration $\ddot{x}_d(t)$ is piecewise-continuous and bounded.*

Two separate user-defined motion and force profiles can be glued together to satisfy Assumption 1 by using the design procedure detailed in Appendix A.

In terms of the exact parameters k_e and b_e , (4) can be rewritten as

$$k_e x_d(t) + b_e \dot{x}_d(t) + w_f(t) = F_d(t), \quad \text{for } F_d(t) > 0, \quad (5)$$

with $w_f(t) := (\hat{k}_e - k_e)x_d(t) + (\hat{b}_e - b_e)\dot{x}_d(t)$ a bounded – due to Assumption 1 – perturbation. When the estimates \hat{k}_e and \hat{b}_e are exact, $w_f(t) = 0$ and $x - x_d(t) \rightarrow 0$ implies that $F_e - F_d(t) \rightarrow 0$. When $\hat{k}_e \neq k_e$ and/or $\hat{b}_e \neq b_e$, $w_f(t) \neq 0$ and acts a perturbation in the stability analysis. Since the mapping (5) is only used for the stability analysis and not in the controller (3), the lack of exact knowledge of k_e and b_e will not affect the stability or tracking of the system described by (1)-(3).

The tracking error

$$z = \begin{bmatrix} z_1 \\ z_2 \end{bmatrix} := \begin{bmatrix} x_d(t) - x \\ \dot{x}_d(t) - \dot{x} \end{bmatrix} \quad (6)$$

can be used to rewrite the closed-loop system dynamics (1)-(3) and (5) as the following perturbed switched system

$$\Sigma^p : \quad \dot{z} = A_i z + N w_i(t) = \begin{bmatrix} 0 & 1 \\ -K_i & -B_i \end{bmatrix} z + N w_i(t), \quad z \in \Omega_i(t), i \in \{1, 2\}, \quad (7)$$

where $N = [0, 1]^T$ and

$$K_1 := \frac{k_p}{M}, \quad B_1 := \frac{k_d + b}{M}, \quad (8a)$$

$$K_2 := \frac{(1 + k_f)k_e}{M}, \quad B_2 := \frac{(1 + k_f)b_e + b_f + b}{M}, \quad (8b)$$

$$w_1(t) := \frac{M - M_a}{M} \ddot{x}_d(t) + \frac{b}{M} \dot{x}_d(t), \quad (8c)$$

$$w_2(t) := \ddot{x}_d(t) + \frac{b_f + b}{M} \dot{x}_d(t) - \frac{1}{M} w_f(t), \quad (8d)$$

with w_f as in (5). The perturbations $w_i(t)$, $i = \{1, 2\}$, are bounded due to Assumption 1. All system parameters are positive, implying that in (7), for $i \in \{1, 2\}$, $K_i, B_i > 0$ and A_i is Hurwitz. The environment is located at $x = 0$, so switching occurs at $x = x_d(t) - z_1 = 0$. Expressed in the z -coordinates, the free motion and contact subspaces, respectively denoted by Ω_1 and Ω_2 , are time-varying: $\Omega_1(t) := \{z \in \mathbb{R}^2 | x_d(t) - z_1 \leq 0\}$ and $\Omega_2(t) := \{z \in \mathbb{R}^2 | x_d(t) - z_1 > 0\}$. Note that for all t , $\Omega_1(t) \cup \Omega_2(t) = \mathbb{R}^2$ and $\Omega_1(t) \cap \Omega_2(t) = \emptyset$.

The environment stiffness k_e is typically much higher than the control gain k_p . Furthermore, the true value of k_e and b_e are usually unknown and therefore the control parameters cannot be selected to result in $K_1 = K_2$ and $B_1 = B_2$ in (7). Thus, in general, Σ^p in (7) represents a switched system. The stability of Σ^p does not follow from the stability of each of the two continuous subsystems (corresponding to free motion and contact) taken separately, as shown, e.g., in [8,10] (see also [23] in the scope of generic switched systems). Hence, the switching between the two subsystems, corresponding to making and breaking contact, must also be taken into account. This is the purpose of the next section.

3 Stability analysis

In this section, sufficient conditions are provided under which Σ^p in (7) is input-to-state stable (ISS) with respect to the input $w_i(t)$, $i = \{1, 2\}$. Note that $w_i(t)$ depends on $x_d(t)$, thereby encoding the information of $F_d(t)$ during the contact phases.

The following definitions, taken from [24], are required for the stability analysis.

Definition 1 Consider a region $\mathcal{T}_i \subset \mathbb{R}^2$. If $z \in \mathcal{T}_i$ implies $cz \in \mathcal{T}_i$, $\forall c \in (0, \infty)$ and $\mathcal{T}_i \setminus \{0\}$ is connected, then \mathcal{T}_i is a **cone**.

Definition 2 Let $\dot{z} = A_i z$ be the dynamics on an open cone $\mathcal{T}_i \subset \mathbb{R}^2$, $i = 1, \dots, m$. An **eigenvector** of A_i is **visible** if it lies in $\overline{\mathcal{T}_i}$, the closure of \mathcal{T}_i .

As a stepping stone towards proving ISS of (7), we provide sufficient conditions for the global uniform exponential stability (GUES) of the origin of Σ^p when $w_i \equiv 0$. This corresponds to studying the unperturbed system

$$\Sigma^u : \quad \dot{z} = A_i z \quad \forall z \in \Omega_i(t). \quad (9)$$

The GUES of the origin of Σ^u for any $x_d(t)$ satisfying Assumption 1 can be concluded by considering the worst-case switching sequence [23,25]. In this way, we obtain the time-invariant system Σ^w , defined below, with state-based switching, that represents the worst-case switching sequence for Σ^u in (9). The worst-case switching sequence is defined as the switching sequence that results in the slowest convergence (or fastest divergence) of the

solution of Σ^u towards (or from) the origin. Denote with $\sigma(t) : \mathbb{R} \rightarrow \{1, 2\}$ the switching sequence corresponding to $i \in \{1, 2\}$ in (9). Note that $\sigma(t)$ depends on the initial condition $z(t_0) = z_0$. Then, the solution of Σ^u starting from z_0 at t_0 will be denoted by $z(t) = \Phi_u(t, t_0; \sigma) z_0$, with $\Phi_u(t, t_0; \sigma)$ the state transition matrix associated with the switching sequence $\sigma(t)$. For $K_2 > K_1$, representing a manipulator interacting with a stiff environment, the worst-case dynamical system Σ^w , associated with the worst-case switching sequence, is characterized by the following lemma.

Lemma 1 Consider the switched system

$$\Sigma^w : \quad \dot{z} = A_i z, \quad \forall z \in \mathcal{S}_i, \quad (10)$$

with A_1 and A_2 as in (7). Assume $K_2 > K_1$ and let

$$\begin{aligned} \mathcal{S}_1 &= \{z \in \mathbb{R}^2 | z_2((K_1 - K_2)z_1 + (B_1 - B_2)z_2) \leq 0\}, \\ \mathcal{S}_2 &= \{z \in \mathbb{R}^2 | z_2((K_1 - K_2)z_1 + (B_1 - B_2)z_2) > 0\}. \end{aligned}$$

For the solution of Σ^u in (9) corresponding to an arbitrary switching signal $\sigma(t)$ and initial condition z_0 , $\|\Phi_u(t, t_0; \sigma) z_0\| \leq \|\Phi_w(t, t_0) z_0\|$ for $t \geq t_0$, where Φ_w denotes the state transition matrix of Σ^w in (10). In this sense, we will refer to $\Phi_w(t, t_0) z_0$, $t \geq t_0$, as the worst-case response of Σ^u with initial condition z_0 .

Proof: Let $\dot{z} = A_{\sigma(t)} z$ denote the time-varying vector field associated with the switching signal $\sigma(t) \in \{1, 2\} \forall t$ corresponding to an arbitrary $x_d(t)$ satisfying Assumption 1. Let $V = \frac{1}{2} z^T z$ be a positive definite comparison function, with time derivative $\dot{V} = z^T \dot{z} = z^T A_{\sigma(t)} z$. Let us define $\dot{V}_i := z^T A_i z$ for $i = \{1, 2\}$. Then it holds that $\dot{V} = z^T A_{\sigma(t)} z \leq \max(\dot{V}_1, \dot{V}_2)$. From the structure of A_1 and A_2 in (7), with $K_2 > K_1$, it follows that $\dot{V}_1 > \dot{V}_2$ if $z_2((K_1 - K_2)z_1 + (B_1 - B_2)z_2) < 0$ and vice versa, such that a switching logic based on $i = \arg\max_{j \in \{1, 2\}} \dot{V}_j$, is equivalent with the one in (10). For equal initial conditions z_0 , it follows that $V(\Phi_u(t, t_0; \sigma)) \leq V(\Phi_w(t, t_0))$. Since $V(z) = \frac{1}{2} \|z\|^2$, it follows that $\|\Phi_u(t, t_0; \sigma)\| \leq \|\Phi_w(t, t_0)\|$ and Σ^w generates the worst-case response of Σ^u . \square

From the definition of \mathcal{S}_1 and \mathcal{S}_2 given in Lemma 1, we obtain the two switching surfaces $z_2 = 0$ and $(K_1 - K_2)z_1 + (B_1 - B_2)z_2 = 0$ that characterize the worst-case switching. These switching surfaces and the subsystems of Σ^w that are active between the switching surfaces are visualized in Figure 2 for $K_2 > K_1$ and $B_2 > B_1$.

In Theorem 1 below, necessary and sufficient conditions for the global uniform asymptotic stability (GUAS) of Σ^w are given. We then show in Lemma 2, that GUAS of Σ^w implies GUES of Σ^u and this, in turn, implies ISS of Σ^p w.r.t. w_i for an arbitrary $x_d(t)$ satisfying Assumption 1. This result is given in Theorem 2 at the end of this section and, together with Theorem 1, constitute the main result of this paper. We refer the interested reader to Appendix B for further details about the background

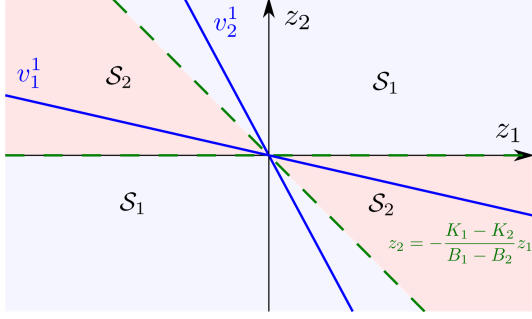


Figure 2. Switching surfaces and domains of Σ^w for $K_2 > K_1$ and $B_2 > B_1$. The vectors v_1^1 and v_2^1 represent the real eigenvectors of A_1 in (14).

material used to obtain the following results.

Theorem 1 Let $K_i, B_i > 0$, $\Delta K := K_1 - K_2 < 0$ and $\Delta B := B_1 - B_2$. The origin of the unperturbed, conewise linear system Σ^w is GUAS if at least one of the following conditions is satisfied:

- i. Σ^w has a visible eigenvector associated with an eigenvalue $\lambda < 0$; in other words, one of the following two conditions is satisfied:
 - (a) a visible eigenvector exists in S_1 , i.e., $\Delta B < 0$, $B_1^2 \geq 4K_1$ and $\frac{\Delta K}{\Delta B} < \frac{2K_1}{B_1 - \sqrt{B_1^2 - 4K_1}}$
 - (b) a visible eigenvector exists in S_2 , i.e., $B_2^2 \geq 4K_2$ and one of the following conditions is satisfied:
 - 1) $\Delta B < 0$ and $\frac{\Delta K}{\Delta B} > \frac{2K_2}{B_2 + \sqrt{B_2^2 - 4K_2}}$, or
 - 2) $\Delta B \geq 0$.
- ii. Σ^w has no visible eigenvectors and $\Lambda_1 \Lambda_2 < 1$, where $\Lambda_i, i = \{1, 2\}$, are given by:
 - 1) if $B_i^2 < 4K_i$,

$$\Lambda_i = \left(\frac{K_i}{\omega_i} \left(\frac{(\Delta K)^2}{L^2} + \frac{Q^2}{4\omega_i^2 L^2} \right)^{-1/2} \right)^{(-1)^i} e^{-\frac{B_i}{2\omega_i} \varphi_i} \quad (11)$$

$$\text{with } \varphi_i := \text{mod} \left(-\arctan\left(\frac{(-1)^i 2\omega_i \Delta K}{Q}\right), \pi \right),$$

$$Q := B_i \Delta K - 2K_i \Delta B, \omega_i := \frac{1}{2} \sqrt{4K_i - B_i^2} \text{ and } L := \sqrt{(\Delta K)^2 + (\Delta B)^2}.$$

- 2) if $B_i^2 = 4K_i$,

$$\Lambda_i = \left| \frac{B_i L}{2\Delta K - B_i \Delta B} \right| e^{((-1)^i \frac{2\Delta K}{2\Delta K - B_i \Delta B})}. \quad (12)$$

- 3) if $B_i^2 > 4K_i$,

$$\Lambda_i = \left| \frac{\Delta K \lambda_{bi} + K_i \Delta B}{K_i L} \right|^{((-1)^i \frac{\lambda_{ai}}{\lambda_{bi} - \lambda_{ai}})} \cdot \left| \frac{\Delta K \lambda_{ai} + K_i \Delta B}{K_i L} \right|^{((-1)^i \frac{\lambda_{bi}}{\lambda_{ai} - \lambda_{bi}})} \quad (13)$$

$$\text{with } \lambda_{ai} := \frac{-B_i - \sqrt{B_i^2 - 4K_i}}{2} \text{ and } \lambda_{bi} := \frac{-B_i + \sqrt{B_i^2 - 4K_i}}{2}.$$

Proof: From Lemma 3 in Appendix B it follows that Σ^w in (10) has no sliding modes on the switching surfaces. Therefore, Theorem 3 can be applied to conclude GUAS of the origin of Σ^w . To this end, consider the conditions under points i and ii sequentially:

- i. Since $K_i, B_i > 0$, both A_1 and A_2 are Hurwitz, such that $\Re(\lambda_{1,2}^i) < 0$, with $\lambda_{1,2}^i = \frac{-B_i \pm \sqrt{B_i^2 - 4K_i}}{2}$ being the eigenvalues of A_i . An eigenvector is visible in S_i if the eigenvalues $\lambda_{1,2}^i$ of A_i are real and for at least one of the corresponding eigenvectors

$$v_1^i := \begin{bmatrix} \frac{-B_i + \sqrt{B_i^2 - 4K_i}}{2K_i} \\ 1 \end{bmatrix}, v_2^i := \begin{bmatrix} \frac{-B_i - \sqrt{B_i^2 - 4K_i}}{2K_i} \\ 1 \end{bmatrix} \quad (14)$$

it holds that $v_j^i \in S_i$, with $j = 1$ or $j = 2$. These eigenvectors lie in the second and fourth quadrant of the phase portrait. For $j = 1$, Figure 2 shows the eigenvectors v_1^1 and v_2^1 and switching surfaces $z_2 = 0$ and $z_2 = -\frac{K_1 - K_2}{B_1 - B_2} z_1$. The subsystem active in S_1 has a visible eigenvector if $\Delta B < 0$ (switching surface in second and fourth quadrant) and the slope of the corresponding real eigenvector with the steepest slope, i.e. v_1^1 , is steeper than $z_2 = -\frac{K_1 - K_2}{B_1 - B_2} z_1$, i.e. the inequalities of condition i.(a) of the theorem hold.

Similarly, it follows that the subsystem active in S_2 has a visible eigenvector if either 1) $\Delta B < 0$ (switching surface in second and fourth quadrant) and $z_2 = -\frac{K_1 - K_2}{B_1 - B_2} z_1$ has a steeper slope than the real eigenvector of S_2 with the least steep slope, i.e. v_2^2 , or 2) $\Delta B \geq 0$ (switching surface in first and third quadrant, hence S_2 spans at least the whole second and fourth quadrant). These two cases hold when conditions 1) and 2) of condition i.(b) of the theorem are satisfied. For both cases, GUAS of the origin follows from case (i) of Theorem 3 in Appendix B.

- ii. In case no visible eigenvectors exist, case (ii) of Theorem 3, provided in Appendix B, must hold with $\Lambda := \Lambda_1^2 \Lambda_2^2 < 1$, or equivalently, $\Lambda_1 \Lambda_2 < 1$ in order for the origin of Σ^w to be GUAS. The expressions (11)-(13) follow from the three cases (B.1)-(B.3) of part (ii) of Theorem 3, with the following vectors and matrices

$$\rho_{12}^1 = -\rho_{12}^2 = \begin{bmatrix} 1 \\ 0 \end{bmatrix}, \quad \rho_{21}^1 = \rho_{21}^2 = \frac{1}{L} \begin{bmatrix} \Delta B \\ -\Delta K \end{bmatrix},$$

$$1) P_i = \begin{bmatrix} \frac{-K_i}{\omega_i} & \frac{-B_i}{2\omega_i} \\ 0 & 1 \end{bmatrix}, \quad 2) P_i = \begin{bmatrix} -\frac{2}{B_i} & -\frac{4}{B_i^2} \\ 1 & 0 \end{bmatrix},$$

$$3) P_i = \begin{bmatrix} \frac{\lambda_{ai}}{K_i} & \frac{\lambda_{bi}}{K_i} \\ 1 & 1 \end{bmatrix}. \quad \square$$

This Theorem can be interpreted as follows. If the system Σ^w does not have a visible eigenvector (case *ii*), the response spirals around the origin and visits the regions \mathcal{S}_1 and \mathcal{S}_2 infinitely many times. In such a case, the worst-case system Σ^w switches between free motion and contact, but if $\Lambda < 1$, defined in the proof of Theorem 1, the resulting bouncing behavior is asymptotically stable, implying that the amplitude of the oscillation decays over time. Furthermore, since the trajectory leaves each cone in *finite* time (see Lemma 5 in Appendix B), the time between two switches is fixed and finite, implying that Zeno behavior (infinitely many switches in finite time) of Σ^w is excluded. If Σ^w does have a visible eigenvector with $\lambda < 0$ (case *i*), the response converges to the origin exponentially without leaving the cone (see Lemma 4 in Appendix B). Then, the system does not switch between free motion and contact and bouncing of the manipulator against the environment does not occur.

The following lemma states that GUAS of Σ^w implies GUES of Σ^u .

Lemma 2 *If Σ^w in (10) is GUAS, then the origin of Σ^u in (9) is GUES for arbitrary $x_d(t)$ satisfying Assumption 1.*

Proof: By Lemma 1, $\|\Phi_u(t, t_0; \sigma)z_0\| \leq \|\Phi_w(t, t_0)z_0\|$. So, if the origin of Σ^w is GUAS, then so is the origin of Σ^u for arbitrary $x_d(t)$ satisfying Assumption 1. Then, from Theorem 2.4 of [23] it follows that the origin of Σ^u is GUES for arbitrary $x_d(t)$ satisfying Assumption 1. \square

From Lemma 2, Σ^u is GUES if Σ^w is GUAS, and this last fact is guaranteed when one of the conditions given in Theorem 1 holds true. The following theorem provides conditions for ISS of the perturbed system Σ^p in (7).

Theorem 2 *Consider the perturbed system Σ^p in (7), with piecewise-continuous, bounded input $w_i(t)$. If the origin of the unperturbed system Σ^u in (9) is GUES for arbitrary $x_d(t)$ satisfying Assumption 1, then Σ^p is ISS w.r.t. $x_d(t)$.*

Proof: For an arbitrary switching sequence $\sigma(t) : \mathbb{R} \rightarrow \{1, 2\}$, resulting from arbitrary $x_d(t)$ satisfying Assumption 1, the solution of Σ^p , with initial condition z_0 at t_0 , can be expressed as (see [26], Chapter 1)

$$z(t) = \Phi_u(t, t_0; \sigma)z_0 + \int_{t_0}^t \Phi_u(t, \tau; \sigma) Nw_i(\tau) d\tau. \quad (15)$$

If the origin of Σ^u is GUES, which is guaranteed if the conditions in Lemma 2 are satisfied, $\|\Phi_u(t, t_0; \sigma)\| \leq ce^{-\lambda(t-t_0)}$, for some constants $c, \lambda > 0$. Then, it follows

from (15) that

$$\begin{aligned} \|z(t)\| &\leq \|\Phi_u(t, t_0; \sigma)z_0\| + \left\| \int_{t_0}^t \Phi_u(t, \tau; \sigma) Nw_i(\tau) d\tau \right\| \\ &\leq ce^{-\lambda(t-t_0)} \|z_0\| + c \int_{t_0}^t e^{-\lambda(t-\tau)} \|Nw_i(\tau)\| d\tau \\ &\leq \underbrace{ce^{-\lambda(t-t_0)} \|z_0\|}_{\beta(\|z_0\|, t-t_0)} + \underbrace{\frac{c}{\lambda} \sup_{t_0 \leq \tau \leq t} \|Nw_i(\tau)\|}_{\gamma(\sup_{t_0 \leq \tau \leq t} \|Nw_i(\tau)\|)}. \end{aligned}$$

Since β is a class \mathcal{KL} function and γ is a class \mathcal{K} function, Σ^p is ISS for arbitrary $x_d(t)$ satisfying Assumption 1. \square

This theorem can be interpreted as follows. If $Nw_i(t) \equiv 0$, the response of Σ^p is equivalent to the response of Σ^u , whose origin is GUES. Due to (5), $x_d(t)$ encodes the information of $F_d(t)$ during the contact phase, so $x \rightarrow x_d(t)$ and $F_e \rightarrow F_d(t)$ exponentially. If $Nw_i(t) \neq 0$, the response of Σ^p deviates from the response of Σ^u , (i.e. x and F_e will only converge to neighbourhoods of $x_d(t)$ and $F_d(t)$, respectively), but due to the ISS property the response of Σ^p is bounded and the bound on the error norm $\|z\|$, with z defined in (6), will depend on the norm of the perturbation Nw_i .

4 Example with a stiff environment

We now illustrate the use of the developed theory by means of simulations and show the implications of satisfying Theorem 2 on the controller design. Consider a manipulator with $M = 1$ kg and $b = 0$ Ns/m (i.e. no viscous friction is present in the manipulator to help dissipate energy), interacting with an environment with $k_e = 10^6$ N/m and $b_e = 10$ Ns/m. For the control parameters we choose $M_a = 0.8$ kg, $k_p = 4000$, $k_d = 80$, $k_f = 1$ and $b_f = 5$. For this parameter set, the eigenvectors of A_2 in (7) are complex, such that no visible eigenvectors exist in the contact phase (see Definition 2). The eigenvectors of A_1 in (7) are real, but not visible. The response of the system is shown in Figure 3. Although $x_d(t)$ and $F_d(t)$ used for the simulation in Figure 3 are not necessarily worst-case inputs, the value $\Lambda = \Lambda_1^2 \Lambda_2^2 = 10.16$ indicates that the system is *potentially* unstable (the conditions in case *ii* of Theorem 1 are *necessary and sufficient* for stability of Σ^w , since they are based on its exact solution). The controller tracks $x_d(t)$ in free motion, but due to the stiff environment and nonzero impact velocity, a large peak force occurs (see bottom plot in Figure 3). The manipulator bounces then back from the environment and breaks contact. During the 0.15 s of intended contact, the manipulator continues to bounce and is not able (see Figure 3) to track the desired contact force $F_d(t)$, which has a maximum of 7 N. Around 0.27 s the *motion* controller is no longer able to bring the manipulator in contact with the environment due to the relatively large negative derivative term in (3a). The amplitude of the bouncing does decay over time, but Figure 3 clearly illustrates an undesired response. The problem is the lack of damping in contact. Increasing

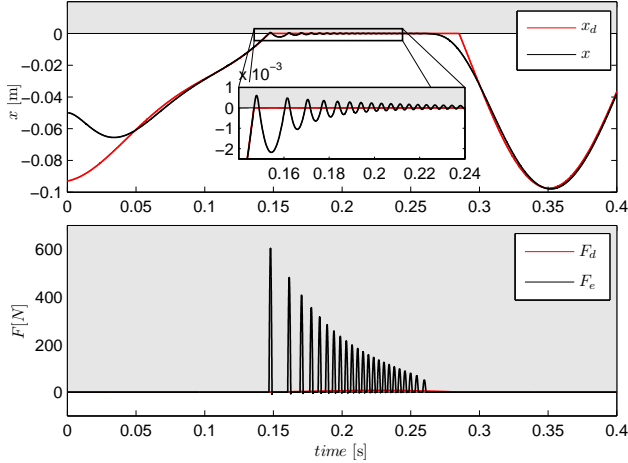


Figure 3. Simulation results with $b_f = 5$. The grey area indicates the contact phase.

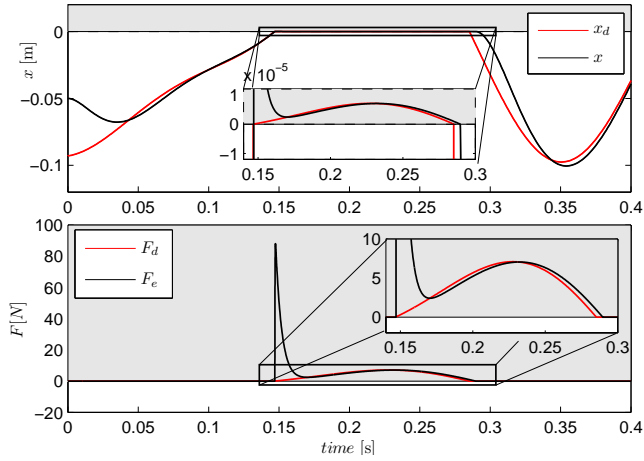


Figure 4. Simulation results with $b_f = 9000$. The grey area indicates the contact phase.

the damping level in the force controller to $b_f = 9000$ results in $\Lambda = \Lambda_1^2 \Lambda_2^2 = 0.98$, such that the origin of Σ^w is GUAS (see Theorem 1) and the system Σ^p is ISS, for *any* motion-force profile $x_d(t)$, $F_d(t)$ satisfying Assumption 1 (see Theorem 2). With $b_f = 9000$, the manipulator does not bounce against the environment (see Figure 4) and, after the peak impact force, the contact force F_e approximately tracks $F_d(t)$.

However, such a high damping gain b_f in contact is probably not realizable in practice, so therefore we propose a different solution, namely a compliant manipulator. The results of Theorem 2 are then used as a systematic procedure to design the stiffness of the wrist. This solution is discussed in the next section.

5 Compliant manipulator design

This section discusses the motivation for the need of a compliant manipulator and shows how Theorem 2 can be used to tune the stiffness and damping properties of the introduced compliancy.

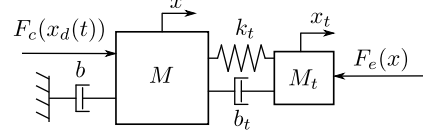


Figure 5. Manipulator with compliant wrist.

5.1 Motivation and design

A drawback of the high damping gain b_f used in the simulation in Figure 4 is that it results in a lag in tracking $F_d(t)$ for $t \in [0.17, 0.28]$ (sluggish response). Moreover, most manipulators are not equipped with velocity sensors. So typically, the velocity signal \dot{x} , used in (3b), must be obtained from the position measurements. Due to measurement noise, encoder quantization and a finite sample interval, realizing the damping force $-b_f \dot{x}$ appearing in (3b) is very hard, for not saying impossible, in practice, even if one would use a state observer to estimate \dot{x} .

Inspired by the favorable properties of the skin around a human finger, we propose, as a more practical alternative, to design the manipulator by including passive compliance in the connection between the arm and the end-effector (wrist) as sketched in Figure 5. Indicating with k_t and b_t , respectively, the stiffness and damping coefficient of the wrist and with x_t the position of the end-effector, the dynamics of the compliant manipulator is

$$M\ddot{x} + b\dot{x} = F_c - F_t, \quad (16a)$$

$$M_t\ddot{x}_t = F_t - F_e(x_t, \dot{x}_t), \quad (16b)$$

where the internal force F_t is given by

$$F_t = k_t(x - x_t) + b_t(\dot{x} - \dot{x}_t). \quad (17)$$

The environment model and controller are still given by (2) and (3), respectively, and (3) controls x to $x_d(t)$.

The compliant wrist and end-effector are designed to improve the response during and after the impact phase. So, we consider a design where the mass M_t is smaller than M to reduce the kinetic energy of M_t engaged at impact. The damping b_t is larger than b_e to help dissipate the impact energy and provide more damping in the contact phase. The stiffness k_t is designed smaller than k_e (k_e is much larger than all other parameters) to reduce the eigenfrequency and increase the damping ratio of the contact phase. In symbols, we can write these assumptions as

$$M_t \ll M, \quad k_t \ll k_e, \quad b_t \gg b_e, \quad \text{and} \quad \frac{b_t}{k_e} \ll 1 \text{ s}. \quad (18)$$

5.2 Reduced order model

The stability results of Section 3 only apply to two-dimensional systems. The dynamics of the 2-DOF compliant manipulator of (16) is 4-dimensional, so Theorem 1 cannot be applied directly. However, when (18)

is satisfied, the compliant 2-DOF manipulator (16) exhibits a clear separation between fast and slow dynamics. In free motion, the fast dynamics are related to $x - x_t$, and, in contact, to the end-effector position x_t . The time-scale of the (exponentially stable) fast dynamics is very small compared to the time-scale of interest, so the slow dynamics can be considered as the dominant dynamics describing the response x of the compliant manipulator to the control input $F_c(t)$.

Consider the 2-DOF compliant manipulator (16), (2) with $M \sim 10^0$, $b \sim 10^0$, $M_t \sim 10^{-2}$, $k_t \sim 10^4$, $b_t \sim 10^2$, $k_e \sim 10^6$ and $b_e \sim 10^1$. The model reduction analysis in Appendix C shows that the slow time-scale response of this system in free motion and contact considered separately can be approximated by the following model of reduced (2nd) order:

$$M\ddot{x} + b\dot{x} = F_c - \bar{F}_e(x, \dot{x}), \quad (19)$$

$$\bar{F}_e(x, \dot{x}) = \begin{cases} 0 & \text{for } x \leq 0 \\ \bar{b}_e\dot{x} + \bar{k}_e x & \text{for } x > 0 \end{cases} \quad (20)$$

with $\bar{b}_e := b_t \frac{k_e}{k_t + k_e}$ and $\bar{k}_e := k_t \frac{k_e}{k_t + k_e}$. The fraction $\frac{k_e}{k_t + k_e} \approx 1$ for $k_t \ll k_e$, so k_t and b_t directly influence the perceived environment damping and stiffness by the mass M .

The reduced-order dynamics (19), (20) are obtained separately for the free motion and contact case. During free motion to contact transitions, the high-frequency dynamics of (16), (2), which are not captured in (19), (20), might still be excited. However, the simulations provided in Section 5.4 indicate that the response of (19), (20) accurately approximates the response of (16), (2), subject to (18) and controlled by (3). Hence, we claim that the reduced-order model (19), (20) can be used to analyze stability of (16), (2), in closed loop with (3).

5.3 Stability of the reduced-order model

Since the reduced-order model (19), (20) has exactly the same structure as (1), (2), we can employ the stability analysis as in Section 3 to design the parameters of the controller in (3). In contact, we use a similar expression to relate $F_d(t)$ to $x_d(t)$, namely

$$F_d(t) = \bar{k}_e x_d(t) + \bar{b}_e \dot{x}_d(t) + \bar{w}_f(t), \quad \text{for } F_d(t) > 0 \quad (21)$$

with $\bar{w}_f(t) := (\tilde{k}_e - \bar{k}_e)x_d(t) + (\tilde{b}_e - \bar{b}_e)\dot{x}_d(t)$, and \tilde{k}_e and \tilde{b}_e available estimates of \bar{k}_e and \bar{b}_e , respectively. The design of the desired trajectories such that $x_d(t)$ is bounded and twice differentiable is discussed in Appendix A.

The system described by (19), (20), (3) and (21) can be expressed in the form Σ^p of (7), with (8a), (8c), (8d) and

$$K_2 := \frac{(1 + k_f)\bar{k}_e}{M}, \quad B_2 := \frac{(1 + k_f)\bar{b}_e + b_f + b}{M}. \quad (22)$$

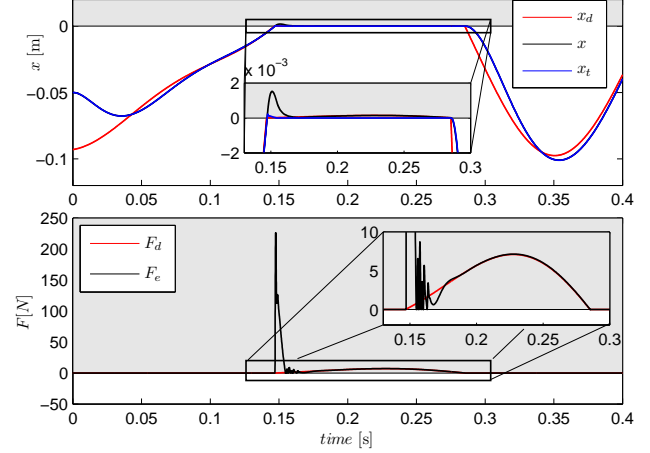


Figure 6. Simulation results of compliant manipulator described by (16). The grey area indicates the contact phase.

As a result, ISS can be concluded from Theorem 2 for arbitrary $x_d(t)$ satisfying Assumption 1 if the conditions of Theorem 1 are satisfied. Compared to the system without compliant wrist, we now have more flexibility to tune the parameters for stability and performance. From Theorem 1 we can compute the required values of the design parameters k_t and b_t to meet design specifications such as the existence of a visible eigenvector corresponding to a stable eigenvalue (implying bounceless impact) or an upper bound on $\Lambda = \Lambda_1^2 \Lambda_2^2$ in Theorem 1. In case of a visible eigenvector corresponding to a stable eigenvalue, stable contact with the environment *without* bouncing can be achieved for *all* bounded signals $x_d(t), F_d(t)$.

5.4 Compliant manipulator example

The following example illustrates how to design the compliant wrist parameters M_t , b_t and k_t to improve the closed-loop performance compared to the simulation results of Figure 3. For the design of the end-effector, consider $M_t = 0.05$ kg and $k_t = 5 \cdot 10^4$ N/m ($k_t \ll k_e$, but still large to minimize the spring-travel in the wrist). With $b_f = 5$ Ns/m, we require $b_t > 170$ Ns/m to guarantee that $\Lambda < 1$, such that one of the conditions of Theorem 1 is satisfied. Figure 6 shows the response of the *unreduced* compliant system (16), (3) and (2), with $b_t = 171$ Ns/m. Compared to Figure 3, the peak impact force is reduced. During the first 20 ms of intended contact, the tip makes and breaks contact due to the fast dynamics of (16). After 20 ms the fast dynamics of (16) damp out, the slow dynamics become dominant and the response of (16) converges to that of (19). Hence, F_e tracks the desired trajectory $F_d(t)$ (without a sluggish response as in Figure 4). Since stability is now obtained with a (more practical) passive implementation, there is more freedom in tuning the parameters of the controller in (3).

Finally, Figure 7 shows a comparison of the response of the 4-dimensional compliant manipulator described by (16), (17), (2), controlled by (3), and the 2-dimensional model described by (19), (20), and controlled by (3). The peak impact force of the 2-dimensional model is 30

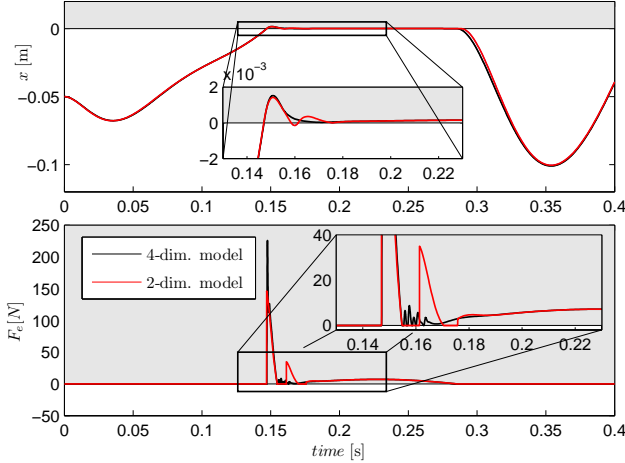


Figure 7. Simulation results of the compliant manipulator described by (16), (17), (2) (black line), and the reduced-order model described by (19), (20) (blue line). The grey area indicates the contact phase, i.e. $x_t > 0$ for the 4-dimensional model (16), (17), (2) and $x > 0$ for the 2-dimensional model (19), (20).

percent smaller, but the time of making and breaking contact is almost equal. The main difference between the two models is found between 0.155 s and 0.18 s, where the fast dynamics of the 4-dimensional model are excited due to bouncing of the tip against the environment. Here, the 2-dimensional model has a second peak around 0.16 s due to a larger impact velocity compared to the tip of the 4-dimensional model. After 0.18 s, the response of both models is similar, indicating that (19), (20) is indeed a good (slow time-scale) approximation of (16), (17), (2) and that Theorem 1 can be used as a guideline for the design of damping and stiffness parameters of the compliant wrist and of the switching controller (3).

5.5 Discussion

From the expressions \bar{k}_e and \bar{b}_e in (20) and the results in Figure 6, we see that the compliance in the manipulator can contribute to guaranteeing stability and improve the tracking performance during free motion to contact transitions. In fact, with $b_t \gg b_e$, the end-effector acts as a vibration-absorber, dissipating the kinetic energy present at impact. And due to the compliance, we can lower the stiffness and increase the damping of the perceived manipulator-environment connection in contact. As a result, the controllers (3a) and (3b) can be tuned separately for optimal performance in free motion and contact, respectively, rather than a trade-off to guarantee stability during transitions in case of a rigid manipulator. Using a light end-effector and tuning of b_t and k_t to satisfy Theorem 1, stable contact with the environment can be made for arbitrary $x_d(t)$ and $F_d(t)$ satisfying Assumption 1. Moreover, if a visible eigenvector exists in the contact phase, even bouncing of the manipulator can be prevented for arbitrary $x_d(t)$ and $F_d(t)$.

6 Conclusion

We consider the position-force control of a manipulator in contact with a stiff environment, focusing on a single direction of contact interaction. We propose a novel switching controller that, when tuned properly, ensures stable bounded tracking of *time-varying* motion and force profiles. Moreover, we provide sufficient conditions for the input-to-state stability (ISS) of the closed-loop tracking error dynamics with respect to perturbations. The stability analysis that we introduce in this paper shows that for realistic parameter values, a high level of controller damping is required during contact to guarantee stability of the closed-loop system. Such high-gain velocity feedback is undesirable for achieving satisfying tracking performance and, moreover, likely unrealizable in practice. Based on the results of our investigation, we propose to combine the proposed switching controller with a mechanical design of the manipulator that includes a compliant wrist. The stability conditions presented in Theorems 1 and 2 can be used as a guideline for the design of the damping and stiffness of this compliant wrist as well as the control parameters to guarantee stability. Furthermore, by designing the closed-loop response to possess visible eigenvectors, those stability conditions can be used to shape the closed-loop response to prevent persistent bouncing of the manipulator against the environment for arbitrary desired motion and force profiles.

References

- [1] B. Siciliano and O. Khatib, editors. *Springer Handbook of Robotics*. Springer-Verlag Berlin, 2008. Ch. 7. Force Control.
- [2] N. Hogan. On the stability of manipulators performing contact tasks. *IEEE J. Robot. Autom.*, 4:677–686, 1988.
- [3] R. Volpe and P. Khosla. A theoretical and experimental investigation of impact control for manipulators. *Int. J. of Robotics Research*, 12:351–365, 1993.
- [4] C. Canudas de Wit and B. Brogliato. Direct adaptive impedance control including transition phases. *Automatica*, 33:643–649, 1997.
- [5] S. Jung, T.C. Hsia, and R.G. Bonitz. Force tracking impedance control of robot manipulator under unknown environment. *IEEE Tr. on Control Systems Technology*, 12(3):474–483, May 2004.
- [6] R. Zovotic Stanisic and Á Valera Fernández. Adjusting the parameters of the mechanical impedance for velocity, impact and force control. *Robotica*, 30:583–597, 2012.
- [7] S.S. Ge, W. Li, and C. Wang. Impedance adaptation for optimal robotenvironment interaction. *Int. J. of Control*, 87:249–263, 2014.
- [8] M.H. Raibert and J.J. Craig. Hybrid position/force control of manipulators. *ASME J. Dyn. Syst. Meas. Contr.*, 103:126–133, 1981.
- [9] O. Khatib. A unified approach for motion and force control of manipulators: The operational space formulation. *IEEE J. Robot. Autom.*, 3:43–53, 1987.
- [10] S. Chiaverini and L. Sciacivco. The parallel approach to force/position control of robotic manipulators. *IEEE Tr. on Robotics and Automation*, 9:361–373, 1993.

- [11] T.-J. Tarn, Y. Wu, N. Xi, and A. Isidori. Force regulation and contact transition control. *IEEE Control Systems Magazine*, 16:32–40, 1996.
- [12] Z. Doulgeri and G. Iliadis. Contact stability analysis of a one degree-of-freedom robot using hybrid system stability theory. *Robotica*, 23:607–614, 2005.
- [13] R. Carloni, R.G. Sanfelice, A.R. Teel, and C. Melchiorri. A hybrid control strategy for robust contact detection and force regulation. In *Proc. of the 2007 American Control Conference*, pages 1461 – 1466, New York City, USA, 2007.
- [14] P.R. Pagilla and B. Yu. A stable transition controller for constrained robots. *IEEE/ASME Tr. on Mechatronics*, 6:65–74, 2001.
- [15] Y.P. Lai, Y.L. anf Li, N.D. Vuong, T.M. Lim, C.Y. Ma, and C.W. Lim. Nonlinear damping for improved transient performance in robotics force control. In *IEEE/ASME Int. Conf. on Advanced Intelligent Mechatronics*, pages 134–139, Kaohsiung, Taiwan, July 2012.
- [16] B. Brogliato. *Nonsmooth Mechanics*. Springer-Verlag London, 1999.
- [17] R. Leine and N. van de Wouw. *Stability and Convergence of Mechanical Systems with Unilateral Constraints*. Springer-Verlag Berlin Heidelberg, 2008.
- [18] P.R. Pagilla. Control of contact problem in constrained Euler-Lagrange systems. *IEEE Tr. on Automatic Control*, 46:1595–1599, 2001.
- [19] B. Brogliato, S.-I. Niculescu, and P. Orhant. On the control of finite-dimensional mechanical systems with unilateral constraints. *IEEE Tr. on Automatic Control*, 42:200–215, 1997.
- [20] J.-M. Bourgeot and B. Brogliato. Tracking control of complementary Lagrangian systems. *Int. J. Bifurcations and Chaos*, 15:1839–1866, 2005.
- [21] I.C. Morărescu and B. Brogliato. Trajectory tracking control of multiconstraint complementary Lagrangian systems. *IEEE Tr. on Automatic Control*, 55:1300–1313, 2010.
- [22] M.W. Spong, S. Hutchinson, and M. Vidyasagar. *Robot modeling and control*. John Wiley & Sons, 2006.
- [23] D. Liberzon. *Switching in Systems and Control*. Birkhäuser Boston, 2003.
- [24] J.J.B. Biemond, N. van de Wouw, and H. Nijmeijer. Nonsmooth bifurcations of equilibria in planar continuous systems. *Nonlinear analysis: Hybrid Systems*, 4:451–474, 2010.
- [25] M. Margaliot. Stability analysis of switched systems using variational principles: an introduction. *Automatica*, 42:2059–2077, 2006.
- [26] Z. Sun and S.S. Ge. *Switched Linear Systems, Control and Design*. Springer-Verlag London, 2005.
- [27] R.I. Leine and H. Nijmeijer. *Dynamics and bifurcations of non-smooth mechanical systems*. Springer-Verlag Berlin Heidelberg, 2004.
- [28] Hassan K. Khalil. *Nonlinear Systems*. Prentice Hall, 2002.
- [29] A.N. Tikhonov, A.B. Vasil’eva, and A.G. Sveshnikov. *Differential equations*. Springer-Verlag Berlin Heidelberg, 1985.

Appendix

A Design of continuous signals $x_d(t)$ and $\dot{x}_d(t)$

In this appendix, we present a method to obtain continuous signals $x_d(t)$ and $\dot{x}_d(t)$ (and corresponding

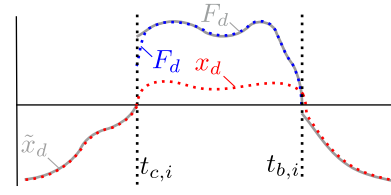


Figure A.1. Example of a construction of $x_d(t)$ and $F_d(t)$ from $\tilde{x}_d(t)$ and $\tilde{F}_d(t)$.

$F_d(t)$), required as reference signals for the switched controller (3), from the continuous and bounded reference profiles $\tilde{x}_d(t)$ and $\tilde{F}_d(t)$ specified by the user.

Denote the i^{th} intended time of making contact by $t_{c,i}$ and the subsequent time of breaking contact by $t_{b,i}$ respectively, as indicated in Figure A.1. Then, during the contact time interval $[t_{c,i}, t_{b,i}]$, $F_d(t)$ and $x_d(t)$ are obtained from

$$\ddot{y}_1 = -2\gamma_1\dot{y}_1 - \gamma_1^2(y_1 - \tilde{F}_d(t)), \quad (\text{A.1a})$$

$$y_1(t_{c,i}) = \hat{k}_e x_d(t_{c,i}) + \hat{b}_e \dot{x}_d(t_{c,i}),$$

$$\dot{y}_1(t_{c,i}) = \hat{k}_e \dot{x}_d(t_{c,i}) + \hat{b}_e \ddot{x}_d(t_{c,i}),$$

$$\ddot{y}_2 = -\frac{\hat{k}_e}{\hat{b}_e}\ddot{y}_2 + \frac{1}{\hat{b}_e}\dot{y}_1, \quad y_2(t_{c,i}) = x_d(t_{c,i}), \quad (\text{A.1b})$$

$$\dot{y}_2(t_{c,i}) = \dot{x}_d(t_{c,i})$$

with the outputs $F_d(t) = y_1$, $x_d(t) = y_2$ and $\dot{x}_d(t) = \dot{y}_2$ for $t \in [t_{c,i}, t_{b,i}]$. The y_2 -dynamics follow from the time derivative of (4) and guarantee continuity of $x_d(t)$ and $\dot{x}_d(t)$ at $t = t_{c,i}$. The y_1 -dynamics represent a critically damped second-order filter on $\tilde{F}_d(t)$ to guarantee continuity of $F_d(t)$ and $\dot{F}_d(t)$ at $t = t_{c,i}$. As a guideline, the time constant $\gamma_1 > 0$ in (A.1a) is chosen such that the 'bandwidth' of this filter is significantly higher than the frequencies present in $\tilde{F}_d(t)$.

Continuity of the profiles $x_d(t)$ and $\dot{x}_d(t)$ when breaking contact is guaranteed when these profiles during the free motion time interval $[t_{b,i}, t_{c,i+1}]$ are obtained from $\tilde{x}_d(t)$ filtered by the critically damped second-order filter

$$\ddot{y}_3 = -2\gamma_2\dot{y}_3 - \gamma_2^2(y_3 - \tilde{x}_d(t)), \quad y_3(t_{b,i}) = x_d(t_{b,i}), \quad (\text{A.2})$$

$$\dot{y}_3(t_{b,i}) = \dot{x}_d(t_{b,i}),$$

with outputs $x_d(t) = y_3$ and $\dot{x}_d(t) = \dot{y}_3$ for $t \in [t_{b,i}, t_{c,i+1}]$. As for γ_1 in (A.1a), the time constant $\gamma_2 > 0$ in (A.2) is chosen such that the 'bandwidth' of (A.2) is significantly higher than the frequencies typically present in $\tilde{x}_d(t)$.

B GUAS of a conewise linear system

The stability results presented here are based on the results presented in [24] and ultimately lead to the statement of Theorem 3, which is used in the proof of Theorem 1 in the main text of this paper. The results in [24] apply to *continuous*, conewise linear systems. The

conewise linear system Σ^w in (10) is, however, discontinuous. The continuity of the vector field is required in [24] to exclude the existence of unstable sliding modes at the switching surfaces of the conewise linear system. The following lemma shows that Σ^w has no sliding modes at the switching surfaces.

Lemma 3 *For $K_1 - K_2 < 0$, the conewise linear system Σ^w has no sliding mode.*

Proof: The existence of a sliding mode at the two switching surfaces $z_2 = 0$ and $z_2 = -\frac{K_1 - K_2}{B_1 - B_2} z_1$ of Σ^w are considered sequentially:

- Consider the subspace $\{z \in \mathbb{R}^2 | z_1 \geq 0\}$. The normal \mathcal{N}_1 to the switching surface $z_2 = 0$ is given by $\mathcal{N}_1 = [0, 1]^T$. The inner product of the vector fields $A_i z$, $i \in \{1, 2\}$, with \mathcal{N}_1 at the switching surface $z_2 = 0$ reads $\lambda \mathcal{N}_1^T A_i \nu_1 = -\lambda K_i$, where $\nu_1 = [1, 0]^T$ and $\lambda \geq 0$. This inner product has the same sign for both vector fields associated with $i = 1$ and $i = 2$, such that no sliding mode exists at the switching surface $z_2 = 0$, see e.g. [27].
- Consider the subspace $\{z \in \mathbb{R}^2 | z_1 \geq 0\}$. The normal \mathcal{N}_2 to the switching surface $z_2 = -\frac{K_1 - K_2}{B_1 - B_2} z_1$ is given by $\mathcal{N}_2 = \frac{1}{L} [\Delta K, \Delta B]^T$, with $\Delta K := K_1 - K_2$, $\Delta B := B_1 - B_2$ and $L := \sqrt{(\Delta K)^2 + (\Delta B)^2}$. The projection of the vector fields $A_i z$, $i \in \{1, 2\}$, with \mathcal{N}_2 at the switching surface $z_2 = -\frac{K_1 - K_2}{B_1 - B_2} z_1$ read

$$\lambda \mathcal{N}_2^T A_1 \nu_2 = \frac{\lambda}{L^2} ((\Delta K)^2 + K_1 (\Delta B)^2 - B_1 (\Delta K) (\Delta B)),$$

$$\lambda \mathcal{N}_2^T A_2 \nu_2 = \frac{\lambda}{L^2} ((\Delta K)^2 + K_2 (\Delta B)^2 - B_2 (\Delta K) (\Delta B)),$$

where $\nu_2 = \frac{1}{L} [-\Delta B, \Delta K]^T$ and $\lambda \geq 0$. It can be shown that $\lambda \mathcal{N}_2^T A_1 \nu_2 - \lambda \mathcal{N}_2^T A_2 \nu_2 = 0$, $\forall K_i, B_i > 0$, hence, the inner products $\lambda \mathcal{N}_2^T A_1 \nu_2$ and $\lambda \mathcal{N}_2^T A_2 \nu_2$ have the same sign, such that no sliding mode exists on the switching surface $z_2 = -\frac{K_1 - K_2}{B_1 - B_2} z_1$, see e.g. [27].

With a similar analysis, the same results can be obtained for the subspace $\{z \in \mathbb{R}^2 | z_1 \leq 0\}$. \square

The following lemma holds for continuous conewise linear systems Σ^w with visible eigenvectors.

Lemma 4 ([24]) *Consider a continuous, conewise linear system of the form Σ^w . When this system contains one or more visible eigenvectors, then $z = 0$ is an asymptotically stable equilibrium of Σ^w if and only if all visible eigenvectors correspond to eigenvalues $\lambda < 0$.*

This lemma can also be shown to be valid for discontinuous conewise systems Σ^w in the absence of a sliding mode. The following lemma is useful in the analysis of the behavior of Σ^w in the absence of visible eigenvectors.

Lemma 5 ([24]) *Let $\tilde{\mathcal{S}}_i$ be a closed cone in \mathbb{R}^2 . Suppose no eigenvectors of $A_i \in \mathbb{R}^{2 \times 2}$ are visible in $\tilde{\mathcal{S}}_i$. Then for any initial condition $z_0 \in \tilde{\mathcal{S}}_i$, with $z_0 \neq 0$, there exists a time $t \geq 0$ such that $e^{A_i t} z_0 \notin \tilde{\mathcal{S}}_i$.*

If Lemma 5 holds for all cones, the trajectories exhibit a spiralling response, visiting each region i once per rota-

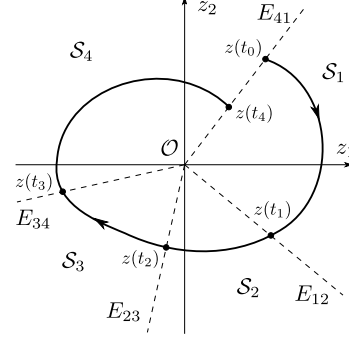


Figure B.1. Example of a trajectory of (10) that traverses each cone once per rotation.

tion, as indicated in Figure B.1. Stability for a spiraling motion can be analyzed by the computation of a return map. Suppose the trajectory of (10) enters a region \mathcal{S}_i at t_{i-1} at position $z(t_{i-1})$, which is located on the boundary $E_{i-1,i}$ between cones \mathcal{S}_{i-1} and \mathcal{S}_i , such that $z(t_{i-1})$ can be expressed as $z(t_{i-1}) = p^i \rho_{i-1,i}$. Here, p^i represents the radial distance from the origin at time t_{i-1} and $\rho_{i-1,i}$ is the unit vector parallel to the boundary $E_{i-1,i}$. The trajectory crosses the next boundary $E_{i,i+1}$ at finite time t_i (Lemma 5), and the position of this crossing is given by $z(t_i) = p^{i+1} \rho_{i,i+1}$, such that $z(t_i)$ is parallel to $\rho_{i,i+1}$. Since the dynamics in each cone are linear, the time t_i can be computed explicitly. The crossing positions are linear in p^i , so expressions for a scalar Λ_i , such that $p^{i+1} = \Lambda_i p^i$, can be obtained.

In order to construct the return map, consider for each cone the following coordinate transformation

$$\tilde{z}^i = P_i^{-1} z, \text{ for } \tilde{z}^i \in \tilde{\mathcal{S}}_i := \{\tilde{z}^i \in \mathbb{R}^2 | \tilde{z}^i = P_i^{-1} z | z \in \mathcal{S}_i\},$$

where P_i is given by the real Jordan decomposition of A_i , yielding $A_i = P_i J_i P_i^{-1}$. Depending on the eigenvalues of A_i , three different cases can be distinguished.

- (1) A_i has complex eigenvalues denoted by $a_i \pm \omega_i$, where a_i and ω_i are real constants and $\omega_i > 0$. Then, $J_i = \begin{bmatrix} a_i & -\omega_i \\ \omega_i & a_i \end{bmatrix}$. Define $\phi(r_1, r_2)$ to be the angle in counter clockwise direction from vector r_1 to vector r_2 . Then,

$$\Lambda_i = \frac{\|\tilde{\rho}_{i-1,i}^i\|}{\|\tilde{\rho}_{i,i+1}^i\|} e^{\frac{a_i}{\omega_i} \phi(\tilde{\rho}_{i-1,i}^i, \tilde{\rho}_{i,i+1}^i)}, \quad (\text{B.1})$$

with $\tilde{\rho}_{i-1,i}^i := P_i^{-1} \rho_{i-1,i}$ and $\tilde{\rho}_{i,i+1}^i := P_i^{-1} \rho_{i,i+1}$

- (2) A_i has two equal real eigenvalues λ_{ai} with geometric multiplicity 1. Then, $J_i = \begin{bmatrix} \lambda_{ai} & 1 \\ 0 & \lambda_{ai} \end{bmatrix}$ and

$$\Lambda_i = \left| \frac{e_2^T \tilde{\rho}_{i-1,i}^i}{e_2^T \tilde{\rho}_{i,i+1}^i} \right| e^{\lambda_{ai} \left(\frac{e_1^T \tilde{\rho}_{i-1,i}^i}{e_2^T \tilde{\rho}_{i,i+1}^i} - \frac{e_1^T \tilde{\rho}_{i-1,i}^i}{e_2^T \tilde{\rho}_{i-1,i}^i} \right)}, \quad (\text{B.2})$$

where $e_1 := [1, 0]^T$ and $e_2 := [0, 1]^T$.

- (3) A_i has two distinct real eigenvalues λ_{ai} and λ_{bi} . Then, $J_i = \begin{bmatrix} \lambda_{ai} & 0 \\ 0 & \lambda_{bi} \end{bmatrix}$ and

$$\Lambda_i = \left| \frac{e_2^T \tilde{\rho}_{i,i+1}^i}{e_2^T \tilde{\rho}_{i-1,i}^i} \right|^{\frac{\lambda_{ai}}{\lambda_{bi} - \lambda_{ai}}} \left| \frac{e_1^T \tilde{\rho}_{i,i+1}^i}{e_1^T \tilde{\rho}_{i-1,i}^i} \right|^{\frac{\lambda_{bi}}{\lambda_{ai} - \lambda_{bi}}} \quad (\text{B.3})$$

From the scalars Λ_i for each cone \mathcal{S}_i , $i = 1, \dots, m$, the return map between the positions z_k and z_{k+1} of two consecutive crossings of the trajectory $z(t)$ with the boundary E_{m1} can be computed as $z_{k+1} = \Lambda z_k$, where

$$\Lambda = \prod_{i=1}^m \Lambda_i.$$

Theorem 3 below is an extension of Theorem 6 in [24] and provides necessary and sufficient conditions for GUAS of the origin of the discontinuous, conewise linear system Σ^w .

Theorem 3 *Under the assumption that no sliding modes exist, the origin of the discontinuous, conewise linear system Σ^w in (10) is GUAS if at least one of the following conditions is satisfied:*

- (i) *In each cone \mathcal{S}_i , $i = 1, \dots, m$, all visible eigenvectors are associated with eigenvalues $\lambda < 0$.*
- (ii) *In case there exists no visible eigenvector, it holds that $\Lambda < 1$.*

Proof: If no sliding modes exist on the switching surfaces, GUAS of the origin of the discontinuous system Σ^w can be proven similarly to the proof of Theorem 6 in [24] for continuous, conewise linear systems. \square

From Lemma 3 it follows that Σ^w in (10) has no sliding modes on the switching surfaces, so Theorem 3 can indeed be applied to conclude GUAS of the origin of Σ^w .

C Model reduction compliant manipulator

The model (19)-(20) describes the slow dynamics of (16), (17), (2) and is obtained by employing Theorem 11.2 of [28]. With this theorem, the slow dynamics are obtained for an infinite time horizon $t \in [t_0, \infty]$. We will refer to it as *Tikhonov's extended theorem*, since the original theorem of Tikhonov, see e.g. Chapter 7 of [29], only applies on a finite time horizon $t \in [t_0, t_f]$.

Tikhonov's extended theorem is applicable to systems described by (non)linear continuous, possibly time varying, dynamics. The dynamics of (16), (17), (2) are not continuous due to the switch between free motion and contact. Therefore, we consider the model reduction of the free motion ($x_t \leq 0$) and contact ($x_t > 0$) phases separately. The simulation results presented in Section 5 indicate that for the considered parameter values the response of the original compliant manipulator dynamics (16), (17), (2), *including* the transitions between free motion and contact, can be approximated by the dynamics of the reduced-order model (19)-(20).

Below, for both free motion and contact, the reduction of the 4th-order model (16), (17), (2) to the second-order

model (19)-(20) is performed in two steps, where in each step the model is reduced with one order.

Free motion: Consider the following states

$$\begin{aligned} e &:= x - x_t \\ \dot{e} &:= \dot{x} - \dot{x}_t. \end{aligned}$$

The following parameters are used as an example to illustrate the separation of the two distinct time-scales of the system described by (16), (17), (2): $M \sim 10^0$, $b \sim 10^0$, $M_t \sim 10^{-2}$, $k_t \sim 10^4$, $b_t \sim 10^2$, $k_e \sim 10^6$ and $b_e \sim 10^1$. For these parameter values, the dynamics (16), (17), (2) in free motion can be written as

$$\begin{aligned} \ddot{x} &= \underbrace{\frac{1}{M}}_{\sim 10^0} F_c(t) - \underbrace{\frac{b}{M}}_{\sim 10^0} \dot{x} - \underbrace{\frac{k_t}{M}}_{\sim 10^4} e - \underbrace{\frac{b_t}{M}}_{\sim 10^2} \dot{e} \\ \underbrace{\frac{M_t}{(1 + M_t/M)k_t}}_{\sim 10^{-6}} \ddot{e} &= \underbrace{\frac{M_t}{M(1 + M_t/M)k_t}}_{\sim 10^{-6}} F_c(t) - e - \underbrace{\frac{b_t}{k_t}}_{\sim 10^{-2}} \dot{e} \\ &\quad - \underbrace{\frac{M_t b}{M(1 + M_t/M)k_t}}_{\sim 10^{-6}} \dot{x}. \end{aligned}$$

Define $\mu_1 := \frac{M_t}{(1 + M_t/M)k_t} \approx \frac{M_t}{M(1 + M_t/M)k_t} \approx \frac{M_t b}{M(1 + M_t/M)k_t}$ and $\mu_2 := \frac{b_t}{k_t}$. With these parameters, it follows that $\mu_1 \ll \mu_2$, and we obtain the following dynamics

$$\ddot{x} = \frac{1}{M}(F_c(t) - b\dot{x} - k_t e - b_t \dot{e}) \quad (\text{C.2a})$$

$$\mu_1 \ddot{e} = \mu_1 F_c(t) - \mu_1 \dot{x} - e - \mu_2 \dot{e}. \quad (\text{C.2b})$$

Note that x does not appear directly in the right-hand side of (C.2). Therefore, the dynamics of (C.2) are described by the three states (\dot{x}, e, \dot{e}) only.

In the analysis that follows, we consider μ_1 and μ_2 as *singular perturbations* and use Tikhonov's extended theorem twice (once for μ_1 and once for μ_2) to obtain a model of reduced order.

Before proceeding, we first decouple the free response of (C.2) from the forced response (due to $F_c(t)$). To this end, consider the coordinate transformation $\tilde{x} := \dot{x} - \tilde{x}_{F_c}(t)$, where $\tilde{x}_{F_c}(t)$ is defined as the forced response of the slow dynamics of (C.2) (i.e. for $\mu_1 = \mu_2 = 0$) to the continuous and bounded input $F_c(t)$, such that

$$M\ddot{\tilde{x}}_{F_c}(t) + b\dot{\tilde{x}}_{F_c}(t) = F_c(t). \quad (\text{C.3})$$

Note that $\tilde{x}_{F_c}(t)$ and $\dot{\tilde{x}}_{F_c}(t)$ are continuous and bounded since $F_c(t)$ is continuous and bounded. By employing (C.3), the unforced dynamics of (C.2) can be expressed

as

$$\ddot{x} = \frac{1}{M}(-b\dot{x} - k_t e - b_t \dot{e}) \quad (\text{C.4a})$$

$$\mu_1 \ddot{e} = \mu_1 F_c(t) - \mu_1(\dot{\tilde{x}} + \dot{\tilde{x}}_{F_c}(t)) - e - \mu_2 \dot{e}. \quad (\text{C.4b})$$

Since μ_1 is much smaller than all other parameters, we treat it as the vanishing perturbation parameter and use Tikhonov's extended theorem to obtain a model of reduced order that describes the slow dynamics of this system. Consider $y = [y_1, y_2]^T := [\dot{\tilde{x}}, e]^T$ as the states of the slow dynamics $f_1(y, \zeta)$ and $\zeta := \dot{e}$ as the state of the fast dynamics $g_1(t, y, \zeta, \mu_1)$ of (C.4) according to

$$\begin{bmatrix} \dot{y}_1 \\ \dot{y}_2 \end{bmatrix} = \begin{bmatrix} \frac{1}{M}(-by_1 - k_t y_2 - b_t \zeta) \\ \zeta \end{bmatrix} =: f_1(y, \zeta) \quad (\text{C.5a})$$

$$\begin{aligned} \mu_1 \dot{\zeta} &= \mu_1 F_c(t) - \mu_1(y_1 + \dot{\tilde{x}}_{F_c}(t)) - y_2 - \mu_2 \zeta \\ &=: g_1(t, y, \zeta, \mu_1). \end{aligned} \quad (\text{C.5b})$$

For $\mu_1 = 0$, $\zeta = h_1(y) := -\frac{1}{\mu_2}y_2$ is the solution of $0 = g_1(t, y, \zeta, 0)$ for $y \in D_y = \mathbb{R}^2$ and $v_1 := \zeta - h_1(y) \in D_{v1} = \mathbb{R}$. Let us analyze the three conditions of Tikhonov's extended theorem sequentially:

C1. The functions f_1, g_1 , their first partial derivatives with respect to (y, ζ, μ_1) , and the first partial derivative of g_1 with respect to t are continuous and bounded on any compact subset $D_y \times D_{v1}$, since $F_c(t)$ is continuous and bounded. Furthermore, $h_1(y)$ and $[\partial g_1(t, y, \zeta, 0)/\partial \zeta]$ have bounded first partial derivatives and $[\partial f_1(y, h_1(t, y), 0)/\partial y]$ is Lipschitz in y .

C2. The slow dynamics of (C.5)

$$\begin{aligned} \dot{y} = f_1(y, h_1(y)) &= \begin{bmatrix} \frac{1}{M}(-by_1 - k_t y_2 + \frac{b_t}{\mu_2} y_2) \\ -\frac{1}{\mu_2} y_2 \end{bmatrix} \\ &= \begin{bmatrix} -\frac{b}{M} & \frac{b_t}{\mu_2 M} - \frac{k_t}{M} \\ 0 & -\frac{1}{\mu_2} \end{bmatrix} \begin{bmatrix} y_1 \\ y_2 \end{bmatrix} \end{aligned} \quad (\text{C.6})$$

have a *globally* exponentially stable equilibrium point $y = 0$, since $-\frac{b}{M}$ and $-\frac{1}{\mu_2}$, representing the eigenvalues of the system matrix of the linear dynamics in (C.6), are both negative.

C3. With $\mu_1 \frac{dv_1}{dt} = \frac{dv_1}{d\tau_1}$ (i.e. $\tau_1 := \frac{1}{\mu_1}t$) the (linear) boundary-layer system

$$\begin{aligned} \frac{\partial v_1}{\partial \tau_1} &= g_1(t, y, v_1 + h_1(y), 0) = -y_2 - \mu_2(v_1 - \frac{1}{\mu_2}y_2) \\ &= -\mu_2 v_1 \end{aligned} \quad (\text{C.7})$$

has a *globally* exponentially stable equilibrium point at the origin (since $\mu_2 > 0$), uniformly in (t, y) with region of attraction $\mathcal{R}_{v1} = D_{v1} = \mathbb{R}$.

From the conditions above, Tikhonov's extended theorem allows us to conclude that for all $t_0 \geq 0$, initial conditions $y_0 \in D_y$, $\zeta_0 \in D_\zeta := \mathbb{R}$, and sufficiently small $0 < \mu_1 < \mu_1^*$, the singular perturbation problem of (C.5) has a unique solution $y(t, \mu_1)$, $\zeta(t, \mu_1)$ on $[t_0, \infty)$, and

$$\begin{aligned} y(t, \mu_1) - \bar{y}(t) &= \mathcal{O}(\mu_1) \\ \zeta(t, \mu_1) - h_1(\bar{y}(t)) - \hat{v}_1(t/\mu_1) &= \mathcal{O}(\mu_1) \end{aligned}$$

holds uniformly for $t \in [t_0, \infty)$, with initial time t_0 , where $\bar{y}(t)$ and $\hat{v}_1(\tau)$ are the solutions of (C.6) and (C.7), with $\bar{y}(t_0) = y(t_0)$ and $\hat{v}_1(t_0) = \zeta(t_0) + \frac{1}{\mu_2}y_2(t_0)$ respectively. Moreover, given any $t_b > t_0$, there is $\mu_1^{**} \leq \mu_1^*$ such that

$$\zeta_1(t, \mu_1) - h_1(\bar{y}(t)) = \mathcal{O}(\mu_1)$$

holds uniformly for $t \in [t_b, \infty)$ whenever $\mu_1 < \mu_1^{**}$. Hence, on the domain $t \in [t_b, \infty)$, (C.5) can be approximated by (C.6). Rewriting the reduced-order model (C.6) as the time-invariant system

$$\dot{y}_1 = \frac{1}{M}(-by_1 - k_t y_2 + \frac{b_t}{\mu_2} y_2) := f_2(y_1, y_2, \mu_2) \quad (\text{C.8a})$$

$$\mu_2 \dot{y}_2 = -y_2 := g_2(y_2, \mu_2), \quad (\text{C.8b})$$

it becomes clear that $\mu_2 = \frac{b_t}{k_t} \sim 10^{-2}$ is much smaller than all other parameters in (C.8). Hence, we can apply Tikhonov's extended theorem once more with μ_2 considered as the singular perturbation parameter, y_1 the slow dynamics and y_2 the fast dynamics.

The details regarding the reduction step with μ_2 considered as the singular perturbation is performed in a similar fashion as the first reduction step and is therefore omitted here for the sake of brevity. With $y_2 = h_2(y_1) := 0$ the solution of $0 = g_2(y_2, 0)$, the following globally exponentially stable slow dynamics of (C.8) are obtained

$$\dot{y}_1 = f_2(y_1, h_2(y_1), 0) = -\frac{b}{M}y_1. \quad (\text{C.9})$$

With $v_2 := y_2 - h_2(y_1)$ and $\tau_2 := \frac{1}{\mu_2}t$, the boundary-layer system $\frac{\partial v_2}{\partial \tau_2} = g_2(y_1, v_2 + h_2(y_1), 0) = -v_2$ is globally exponentially stable. Hence, the three conditions of Tikhonov's extended theorem are satisfied, such that it can be concluded that (C.9) is an approximation of (C.8). After reversing the coordinate transformation, i.e. $y_1 = \dot{x} - \dot{\tilde{x}}_{F_c}(t)$, and using (C.3), we obtain

$$M\ddot{x} + b\dot{x} = F_c(t) \quad (\text{C.10})$$

as the approximation of (16) in free motion.

Contact: Similar as for the free motion case, the model reduction for the contact case is performed in two steps.

Due to the relatively high environmental contact stiffness k_e in (16), it is expected that x_t (and time derivatives) is approximately equal to zero (the nominal position of the environment). Therefore, the motion x_t of the tip can be considered as the fast dynamics, and the motion x of the manipulator can be considered as the slow dynamics. The dynamics (16), (17), (2) for $x_t > 0$ can be rewritten as

$$\ddot{x} = \underbrace{\frac{1}{M}}_{\sim 10^0} F_c(t) - \underbrace{\frac{(b+b_t)}{M}}_{\sim 10^2} \dot{x} + \underbrace{\frac{b_t}{M}}_{\sim 10^2} \dot{x}_t - \underbrace{\frac{k_t}{M}}_{\sim 10^4} (x - x_t) \quad (\text{C.11a})$$

$$\underbrace{\mu_3}_{\sim 10^{-8}} \ddot{x}_t = \underbrace{\frac{k_t}{k_t + k_e}}_{\sim 10^{-2}} x + \underbrace{\frac{b_t}{k_t + k_e}}_{\sim 10^{-4}} \dot{x} - x_t - \underbrace{\frac{b_t + b_e}{k_t + k_e}}_{\sim 10^{-4}} \dot{x}_t, \quad (\text{C.11b})$$

where $\mu_3 := \frac{M_t}{k_t + k_e}$. Consider the coordinate transformation

$$\begin{aligned} y_1 &:= x - \bar{x}_{F_c}(t), \\ y_2 &:= \dot{x} - \dot{\bar{x}}_{F_c}(t), & \zeta_1 &:= \dot{x}_t - \dot{\bar{x}}_{t,F_c}(t), \\ y_3 &:= x_t - \bar{x}_{t,F_c}(t), \end{aligned} \quad (\text{C.12})$$

such that $y = [y_1, y_2, y_3]^T = 0$ and $\zeta_1 = 0$ is the equilibrium of (C.11) in the new coordinates. In (C.12), $\bar{x}_{t,F_c}(t)$ and $\bar{x}_{F_c}(t)$ are defined as the forced response of (C.11) for $\mu_3 = 0$, to the continuous and bounded input $F_c(t)$, i.e.

$$\dot{\bar{x}}_{t,F_c}(t) = \frac{1}{b_t + b_e} \left(k_t \bar{x}_{F_c}(t) + b_t \dot{\bar{x}}_{F_c}(t) - (k_t + k_e) \bar{x}_{t,F_c}(t) \right), \quad (\text{C.13})$$

$$M \ddot{\bar{x}}_{F_c}(t) + (b + b_t) \dot{\bar{x}}_{F_c}(t) - b_t \dot{\bar{x}}_{t,F_c}(t) + k_t (\bar{x}_{F_c}(t) - \bar{x}_{t,F_c}(t)) = F_c(t). \quad (\text{C.14})$$

Using the coordinate transformation (C.12) and the expressions (C.13) and (C.14), (C.11) can be rewritten as

$$\begin{aligned} \begin{bmatrix} \dot{y}_1 \\ \dot{y}_2 \\ \dot{y}_3 \end{bmatrix} &= \begin{bmatrix} y_2 \\ \frac{1}{M} (-(b+b_t)y_2 + b_t \zeta_1 - k_t(y_1 - y_3)) \\ \zeta_1 \end{bmatrix} \\ &=: f_3(y, \zeta_1) \end{aligned} \quad (\text{C.15a})$$

$$\begin{aligned} \mu_3 \dot{\zeta}_1 &= \frac{1}{k_t + k_e} \left(k_t y_1 + b_t y_2 - (k_t + k_e) y_3 \right. \\ &\quad \left. - (b_t + b_e) \zeta_1 \right) - \mu_3 \ddot{\bar{x}}_{t,F_c}(t) \\ &=: g_3(t, y, \zeta_1, \mu_3). \end{aligned} \quad (\text{C.15b})$$

Since μ_3 is much smaller than all other parameters, see (C.11b), we treat it as the vanishing perturbation and

use Tikhonov's extended theorem to obtain a model of reduced order.

The details regarding the reduction step with singular perturbation parameter μ_3 follows similar to the reduction step for the free motion case with μ_1 considered as the singular perturbation parameter and is therefore omitted for the sake of brevity. With

$$\zeta_1 = \frac{1}{b_t + b_e} (k_t y_1 + b_t y_2 - (k_t + k_e) y_3) =: h_3(y)$$

the solution of $0 = g_3(t, y, \zeta_1, 0)$, the following globally exponentially stable slow dynamics of (C.15) are obtained

$$\begin{aligned} \dot{y} &= f_3(y, h_3(y)) \\ &= \begin{bmatrix} y_2 \\ \frac{1}{M} (-(b+b_t)y_2 + \frac{b_t}{b_t + b_e} (k_t y_1 + b_t y_2 - (k_t + k_e) y_3) - k_t y_1 + k_t y_3) \\ \frac{1}{b_t + b_e} (k_t y_1 + b_t y_2 - (k_t + k_e) y_3) \end{bmatrix} \end{aligned} \quad (\text{C.16})$$

With $v_3 := \zeta_1 - h_3(y) \in D_{v_3} = \mathbb{R}$ and $\mu_3 \frac{dv_3}{dt} = \frac{dv_3}{d\tau_3}$ (i.e. $\tau_3 := \frac{1}{\mu_3} t$), the boundary-layer system

$$\frac{\partial v_3}{\partial \tau_3} = g_3(t, y, v_3 + h_3(y), 0) = -\frac{b_t + b_e}{k_t + k_e} v_3$$

is globally exponentially stable, and the conditions of Tikhonov's extended theorem are satisfied, such that it can be concluded that (C.16) is an approximation of (C.15). Using (C.13), (C.14) and inverting the coordinate transformation (C.12), the (intermediate) slow dynamics (C.16) can be written in the original coordinates as

$$\begin{aligned} M \ddot{x} &= F_c(t) - (b + b_t) \dot{x} - k_t x + k_t x_t \\ &\quad + \frac{b_t}{b_t + b_e} (k_t x + b_t \dot{x} - (k_t + k_e) x_t) \end{aligned} \quad (\text{C.17a})$$

$$(b_t + b_e) \dot{x}_t = k_t x + b_t \dot{x} - (k_t + k_e) x_t. \quad (\text{C.17b})$$

This third-order system is further approximated to a system of order 2 by considering $\mu_4 := \frac{b_t + b_e}{k_t + k_e}$ as a singular perturbation parameter. To this end, consider the state transformation

$$\begin{aligned} y_1 &:= x - \bar{r}(t), \\ y_2 &:= \dot{x} - \dot{\bar{r}}(t), \\ \zeta_2 &:= (k_t + k_e)(x_t - \bar{r}_t(t)), \end{aligned} \quad (\text{C.18})$$

such that $y = [y_1, y_2]^T = 0$ and $\zeta_2 = 0$ is the equilibrium of (C.17) in the new coordinates. Here, $\bar{r}_t(t)$ is defined

as the forced response of the fast dynamics of (C.17) for $\mu_4 = 0$, and $\bar{r}(t)$ is defined as the forced response of the slow dynamics of (C.17) to the input $F_c(t)$, with $\mu_4 = 0$, i.e.

$$\bar{r}_t(t) = k_t \bar{r}(t) + b_t \dot{\bar{r}}(t) \quad (\text{C.19})$$

$$M \ddot{r}(t) + (b + b_t \frac{k_e}{k_t + k_e}) \dot{r}(t) + k_t \frac{k_e}{k_t + k_e} \bar{r}(t) = F_c(t). \quad (\text{C.20})$$

Rewriting (C.17) in terms of the coordinates y_1 , y_2 and ζ_2 , given in (C.18), and using (C.19), (C.20), we obtain

$$\begin{bmatrix} \dot{y}_1 \\ \dot{y}_2 \end{bmatrix} = \begin{bmatrix} y_2 \\ \frac{1}{M} \left(- (b + b_t) y_2 - k_t y_1 + \frac{k_t}{k_t + k_e} \zeta_2 + \frac{b_t}{b_t + b_e} (k_t y_1 + b_t y_2 - \zeta_2) \right) \end{bmatrix} =: f_4(y, \zeta_2) \quad (\text{C.21a})$$

$$\underbrace{\mu_4}_{\sim 10^{-4}} \dot{\zeta}_2 = \underbrace{k_t}_{\sim 10^4} y_1 + \underbrace{b_t}_{\sim 10^2} y_2 - \zeta_2 - \underbrace{\mu_4}_{\sim 10^{-4}} \dot{r}_t(t) := g_4(t, y, \zeta_2, \mu_4). \quad (\text{C.21b})$$

Since μ_4 is small compared to the other parameters, it is considered a singular perturbation parameter for the system (C.21) and Tikhonov's extended theorem is used once more to obtain a model of reduced order. Again, the proof of the reduction step with μ_4 considered as the singular perturbation follows similar to the previous reduction steps and is therefore omitted.

For $\mu_4 = 0$, $\zeta_2 = k_t y_1 + b_t y_2 := h_4(y)$ is the root of $0 = g_4(t, y, \zeta_2, 0)$ and the following slow dynamics of (C.21) are obtained

$$\dot{y} = f_4(y, h_4(y)) = \begin{bmatrix} y_2 \\ \frac{1}{M} \left(- (b + b_t \frac{k_e}{k_t + k_e}) y_2 - k_t \frac{k_e}{k_t + k_e} y_1 \right) \end{bmatrix} \quad (\text{C.22})$$

With $v_4 := \zeta_2 - h_4(y) \in D_{v_4} = \mathbb{R}$ and $\mu_4 \frac{dv_4}{dt} = \frac{dv_4}{d\tau_4}$ (i.e. $\tau_4 := \frac{1}{\mu_4} t$), the boundary-layer system $\frac{\partial v_4}{\partial \tau_4} = g_4(t, y, v_4 + h_4(y), 0) = -v_4$ is globally exponentially stable, and the conditions of Tikhonov's extended theorem are satisfied, such that the theorem allows us to conclude that (C.22) is an approximation of (C.21). Using the inverse of the coordinate transformation (C.18), we obtain

$$M(\ddot{x} - \ddot{r}(t)) = -k_t \frac{k_e}{k_t + k_e} (x - \bar{r}(t)) - (b + b_t \frac{k_e}{k_t + k_e}) (\dot{x} - \dot{\bar{r}}(t)).$$

Using (C.20), the slow dynamics of (C.17) (and thus of (C.11)) are given by

$$M \ddot{x} + b \dot{x} = F_c(t) - k_t \frac{k_e}{k_t + k_e} x - b_t \frac{k_e}{k_t + k_e} \dot{x}. \quad (\text{C.23})$$

Finally, by combining the results (C.10) and (C.23), for free motion and contact, we obtain the model of reduced order described by (19)-(20).